THE JOURNAL OF PHYSICAL CHEMISTRY C

Article

pubs.acs.org/JPCC

First-Principles Study of Lithiation of Type I Ba-Doped Silicon Clathrates

Xihong Peng,[†] Qun Wei,[†,‡] Ying Li,[§] and Candace K. Chan*[,§]

[†]College of Letters and Sciences, Arizona State University, Mesa, Arizona 85212, United States

[‡]School of Physics and Optoelectronic Engineering, Xidian University, Xi'an 710071, People's Republic of China

[§]Materials Science and Engineering, School for Engineering of Matter, Transport and Energy, Arizona State University, Tempe, Arizona 85287, United States

Supporting Information

ABSTRACT: Silicon clathrate materials, previously known for their superconducting and thermoelectric characteristics, have also recently been investigated for their electrochemical properties as anodes for lithium-ion batteries due to their unique cage structure and ability to incorporate extrinsic guest atoms. To better understand the preferred structures for small degrees of lithiation, first-principles density functional theory (DFT) was used to investigate the type I clathrate compounds Si_{46}, $Li_xBa_ySi_{46}$ ($0 \le x \le 8$; $y = 6, 8$), and $Li_xBa_yAl_6Si_{40}$ ($0 \le x \le 8$; $y = 6$). The formation energies, electronic band structures, and density of states (DOS) were calculated. Lithium occupation in framework vacancies, empty and Ba-occupied cage cavities, and near the pentagonal and hexagonal faces of the clathrate polyhedra was considered. The data showed that Li insertion into framework or Ba vacancies could stabilize the clathrate structure. Silicon substitution by Al lowered the formation energies of the lithiated compounds and mitigated the calculated volume increase upon lithiation. The results also showed that it is energetically feasible for multiple guest atoms to be placed in the Si_{24} cages. Changes in the clathrate atomic structure (e.g., bond lengths and angles) and electronic structure were highly dependent on the location of the Li and guest atom spacing within the clathrate framework. The results from this study can elucidate the preferred structural configurations for Li in type I, Ba-doped silicon clathrates and also be informative for efforts related to understanding the structures obtained after electrochemical insertion of lithium into silicon clathrates.

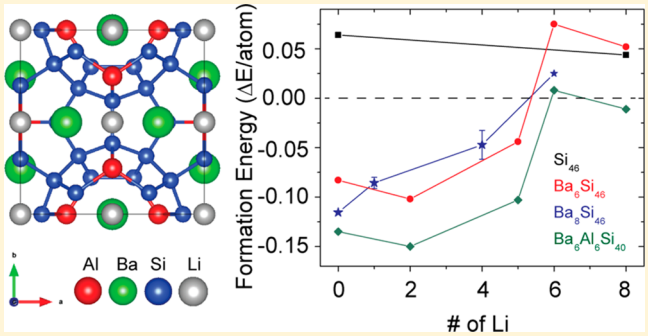

1. INTRODUCTION

Silicon clathrates[1] contain silicon covalently bonded in face-sharing Si_{20}, Si_{24}, and/or Si_{28} clusters and have attracted interest for their electronic (e.g., semiconducting,[2] superconducting,[3−5] thermoelectric[6,7]) and mechanical properties[8,9] resulting from their unique cage-like structures. The polyhedra in silicon clathrates create natural cavities for guests such as alkali and alkaline earth atoms, which can scatter acoustic phonon modes and lower the clathrate thermal conductivity, making them promising materials for thermal energy conversion[4,10] or hydrogen storage.[11,12] The clathrate structure has also been proposed to be useful for energy storage applications. Diamond cubic (c-Si) and amorphous silicon have been extensively studied as high-capacity anode materials[13−15] for Li-ion batteries but suffer from large volume changes and structural transformations, which can affect their long-term cycling stability. In contrast, the polyhedral cavities found in silicon clathrates may be able to provide sufficient space for the insertion of Li ions without affecting the structure of the silicon framework.

Type I clathrates of the form M_8Si_{46} (where M is the guest atom residing within the cage cavities) are made of two pentagonal dodecahedra (Si_{20} cages) plus six tetrakaidecahedra (Si_{24} cages) per unit cell. Type I clathrates adopt a crystal structure belonging to the simple cubic space group $Pm\bar{3}n$ with M atoms located in the 6d (center of the Si_{24} cages) and 2a sites (center of the Si_{20} cages), as described with Wyckoff symmetry notation (Figure 1). Each Si_{24} cage is composed of 12 pentagonal and 2 hexagonal faces, while the Si_{20} cage has only 12 pentagonal faces. On the basis of the accessible volume in the empty type I clathrate Si_{46} (42.9 Å^3/unit cell) and a Li^+ probe sphere with ionic radius of 0.76 Å, an occupancy of 23 Li per unit cell corresponding to a specific capacity of 478 mAh/g was predicted, assuming no volume expansion.[16] However, the difficulty of synthesizing guest-free Si_{46}[17,18] precludes the experimental verification of this result.

On the other hand, type II clathrates of the form M_ySi_{136} ($0 < y < 24$) can be prepared with close to empty cavities. Type II clathrates adopt the face-centered cubic structure $Fd\bar{3}m$ and are composed of 16 Si_{20} cages and eight hexakaidecahedron (Si_{28}

Received: August 3, 2015
Revised: November 19, 2015
Published: November 23, 2015

DOI: 10.1021/acs.jpcc.5b07523
J. Phys. Chem. C 2015, 119, 28247−28257

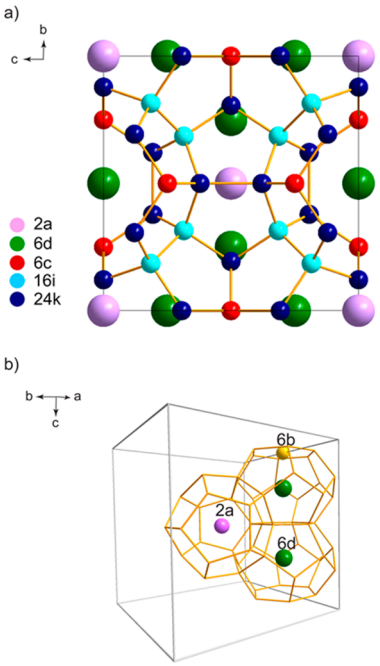

Figure 1. Type I silicon clathrate structures. (a) Ba_8Si_{46} unit cell with crystallographic sites labeled using Wyckoff notation: Ba 6d (green), Ba 2a (pink), Si 6c (red), Si 16i (cyan), Si 24k (blue). (b) Wire-frame representation of Si_{20} and two Si_{24} cages with 2a, 6b, and 6d sites labeled. Other atoms in the unit cell are omitted for clarity.

cages). Experimental investigations showed that electrochemical lithiation of Si_{136} with unfilled (empty) cages[19] as well as cages fully occupied by Na guest atoms[20] was feasible. However, in both cases the clathrate structure was observed to collapse and undergo amorphization upon introduction of large amounts of lithium. Our previous first-principles calculations[20] showed that the formation energies for lithiated type II clathrates were not as low as the formation energy for $Li_{15}Si_4$, which is the fully lithiated phase observed upon electrochemical lithiation of silicon. Calculations performed by Yang and Tse[21] suggested that partial occupation of the type II cage cavities by Ba could help stabilize the Si_{136} structure during lithiation; Ba_8Si_{136} and Ba_6Si_{136} were proposed as potential anode materials that could accept up to 3 Li atoms per Si_{28} cage. However, to our knowledge, there has not been any experimental demonstration of type II clathrates with only partial Ba occupation in the 24 possible guest atom sites, although $Na_{16}Ba_8Si_{136}$ has been synthesized.[22]

In this work, we turn our attention to the Ba-doped type I clathrate structure and evaluate its properties as a Li-ion intercalation material using first-principles density functional theory. Although the type II structure contains the larger Si_{28} cages, it also has a higher fraction of the smaller Si_{20} cages, which could be more susceptible to distortion and structural collapse under Li insertion. To our knowledge, the lithiation properties of type I Ba_ySi_{46} have not been investigated using first-principles methods, and there have not been any detailed studies on the fate of the Si_{24} or Si_{20} cage structure during Li insertion. Furthermore, type I Ba_ySi_{46} compounds can be synthesized using high-pressure techniques[3,23,24] or oxidation of $Ba_4Li_2Si_6$[25] and have been extensively studied for their thermoelectric properties.[3,5,23,26,27] Substitution of the Si framework with other elements such as Al to form ternary compounds can decrease the melting point of the clathrate while preserving the cage structure, which enables synthesis using direct melting rather than high-pressure methods.[7,28,29] We recently experimentally demonstrated that type I clathrates based on $Ba_8Al_zSi_{46-z}$ can be electrochemically lithiated and delithiated.[30] Furthermore, in contrast to type II clathrates and diamond cubic silicon, no evidence of structural collapse or amorphization after lithiation could be discerned in the ternary type I clathrate using X-ray diffraction (XRD) or nuclear magnetic resonance (NMR) spectroscopy. However, the precise location of the inserted Li inside the type I clathrate structure has not yet been identified using structural characterization methods.

Here we present our first-principles investigation of the type I clathrate compounds Si_{46}, $Li_xBa_ySi_{46}$ ($0 \le x \le 8$; $y = 6, 8$), and $Li_xBa_yAl_6Si_{40}$ ($0 \le x \le 8$; $y = 6$) in order to understand the preferred structures for small degrees of lithiation. The formation energies, electronic band structures, and density of states (DOS) were calculated. Different possible Li sites were considered to understand the most energetically stable structures and the effect of Li insertion on the Si−Si bond lengths, bond angles, and overall framework structure.

2. COMPUTATIONAL METHODS

The first-principles density-functional theory (DFT) calculations were performed using the VASP code.[31,32] The PBE functional[33] and projector augmented wave (PAW)[31] potentials were used along with plane wave basis sets. In the PAW potentials, the Si 3s and 3p, Ba 5s, 5p, and 6s, Al 3s and 3p, and Li 1s and 2s electrons were treated as valence electrons. The energy cutoff for the plane wave basis set was 300 eV. The convergence criteria for energy and force were set to be 0.01 and 0.1 meV, respectively. The reciprocal space was sampled using Monkhorst Pack meshes 3 × 3 × 3 centered at the gamma.

The total energies, optimized lattice constants and atomic coordinates, electronic band structure, and DOS of the silicon clathrates were calculated based on the above simulation parameters. The geometry optimization of a clathrate structure was performed in two steps. First, the total volume of the unit cell was optimized without the constraint of cubic symmetry. Then the atomic coordinates of the structure were relaxed within the constraint of cubic symmetry using the optimized volume obtained in the first step. The structure obtained at the end of the first step was found to have a negligible distortion (less than 1% deviation) compared to the structure under cubic constraint (at the end of the second step). Therefore, we reported only cubic cell parameters for the optimized structures.

The formation energies, E_{form}, for the clathrates in eV/atom from the bulk components[2,9] were obtained using eqs 1−4), where E(Si), E(Li), E(Ba), and E(Al) are the total energies per atom for diamond cubic Si, bcc Li, bcc Ba, and fcc Al, respectively. The calculated total energies per atom were found to be −5.417 eV for Si, −1.904 eV for Li, −1.922 eV for Ba, and −3.746 eV for Al. The formation energies enable assessment of the thermodynamic stability of the clathrate structure with respect to the atomic constituents in elemental form. Negative formation energies indicate the structures are more stable than the isolated bulk elements, suggesting that synthesis of the clathrate can be achieved, i.e., from crystallization of a melt containing the bulk sources.[34−36]

DOI: 10.1021/acs.jpcc.5b07523
J. Phys. Chem. C 2015, 119, 28247−28257

Guest-free Si_{46}:

$$E_{form} = \frac{E(Si_{46}) - 46E(Si)}{46} \quad (1)$$

Ba-filled clathrate, e.g., Ba_6Si_{46}:

$$E_{form} = \frac{E(Ba_6Si_{46}) - 46E(Si) - 6E(Ba)}{52} \quad (2)$$

Lithiated clathrate, e.g., $Li_xBa_6Si_{46}$:

$$E_{form} = \frac{E(Li_xBa_6Si_{46}) - xE(Li) - 6E(Ba) - 46E(Si)}{(x + 52)} \quad (3)$$

Ternary clathrate, e.g., $Ba_6Al_6Si_{40}$:

$$E_{form} = \frac{E(Ba_6Al_6Si_{40}) - 6E(Ba) - 6E(Al) - 40E(Si)}{52} \quad (4)$$

The dynamic stabilities of the lithiated clathrate structures were checked using first-principles phonon calculations with a supercell approach as implemented in the Phonopy code.[37,38] The atomic charge of each individual atom in the clathrate was calculated using the Bader scheme[39] to explore the possibility of electron charge transfer among the atoms in the structure.

The average equilibrium lithium potentials were calculated using the equations established by Ceder and colleagues.[40,41] This voltage reflects the difference in chemical potential between the anode and the cathode in an electrochemical cell, in which the anode is delithiated (oxidized) and cathode is lithiated (reduced) during the discharge,[41] as shown in eq 5, where F is Faraday's constant and z is the charge in electrons transported by lithium in the electrolyte (1).

$$V(x) = -\frac{\mu_{Li}^{cathode}(x) - \mu_{Li}^{anode}}{zF} \quad (5)$$

For a half-cell configuration with a Li metal anode and clathrate cathode, $V(x) > 0$ represents the discharge process. The Gibbs free energy change (ΔG_r) for the discharge reaction can be obtained from the total energies as shown in eq 6, using the insertion of 8 Li into Si_{46} as an example.

$$\Delta G_r = E(Li_8Si_{46}) - 8E(Li) - E(Si_{46}) \quad (6)$$

The average lithium potential, $V(x)$, is then obtained using eq 7.

$$V(x) = -\frac{\Delta G_r}{x} \quad (7)$$

The theoretical specific gravimetric capacity, C_G (in mAh/g), was determined using eq 8, where F is Faraday's constant (9.6485×10^4 C), x is the number of Li inserted, and M_w is the molecular weight of the compound.

$$C_G = \frac{1000xF}{3600M_w} \quad (8)$$

3. RESULTS

3.1. Unlithiated Compositions. The Ba_8Si_{46} clathrate structure was generated using the atomic coordinates reported in the literature.[42] Due to the small size of the Si_{20} cages, the slight Ba deficiency observed in Ba-doped type I clathrates[3,23] is thought to be associated with this cage (i.e., the 2a site). For this reason, Ba_6Si_{46} was also considered, in which the 2a sites are empty and available for occupation by Li. $Ba_6Al_6Si_{40}$ was chosen as the Al-substituted clathrate to investigate. Due to the larger covalent radius[43] of Al (1.21 Å) compared to Si (1.11 Å), the substitution of Si with Al increases the framework bond length and clathrate lattice constant.[44] While Al substitution can occur at any of the three crystallographically distinct Si 6c, 16i, and 24k sites[6,44] (Figure 1a), for low degrees of substitution, studies have shown that the 6c site is preferred.[6,45] Hence, the $Ba_6Al_6Si_{40}$ structure was calculated with the 6c sites occupied by Al.

The calculated formation energies and lattice constants for guest free Si_{46} and unlithiated (i.e., $x = 0$) Ba_6Si_{46}, Ba_8Si_{46}, $Ba_6Al_6Si_{40}$ are shown in Figure 2a and 2b, respectively. Guest-

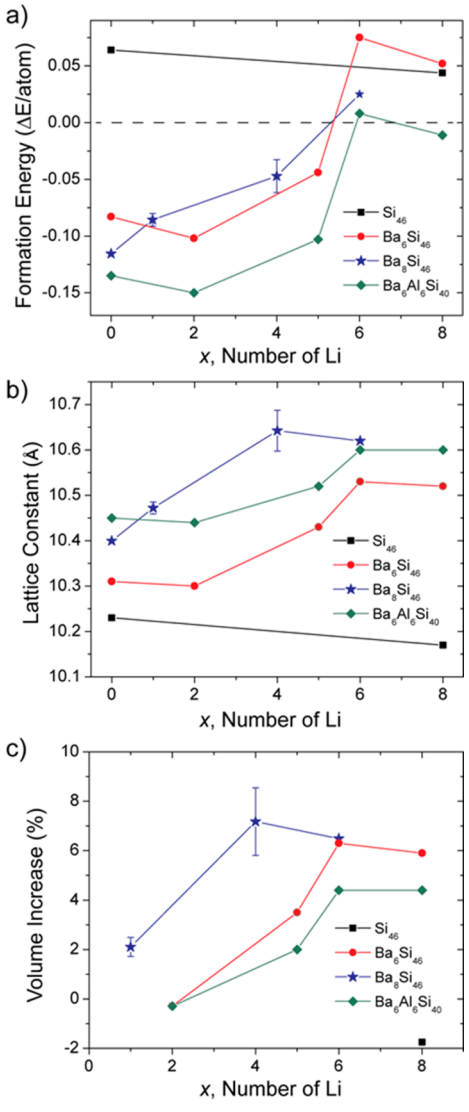

Figure 2. DFT-calculated (a) formation energies and (b) lattice constants for the unlithiated and lithiated clathrates, where the x axis represents the number of Li inserted; (c) calculated volume increase for the lithiated compounds relative to the unlithiated counterparts. For Ba_8Si_{46}, four different clathrate geometry configurations for $x = 1$ and 4 were investigated, as described in the text; the range of values and middle point are shown here, with more details presented in Tables 2 and 3.

DOI: 10.1021/acs.jpcc.5b07523
J. Phys. Chem. C 2015, 119, 28247−28257

free Si_{46} had a slightly positive formation energy of 0.064 eV/atom. The formation energy decreased to −0.083 eV/atom for Ba_6Si_{46} (6d sites occupied by Ba) and −0.116 eV/atom for Ba_8Si_{46} (2a and 6d sites occupied by Ba). The Al-substituted clathrate $Ba_6Al_6Si_{40}$ had an even lower formation energy of −0.135 eV/atom. The lattice constants increased with the introduction of Ba guest atoms and Al substitution (Figure 2b).

3.1. Lithium in the Framework Positions. The first site considered for occupation by Li was at a vacancy in the clathrate framework structure. To our knowledge, the only experimental evidence that Li can occupy a framework vacancy was observed in $K_8Li_xGe_{46-x}$ ($0 \le x \le 2.3$),[46] and it is not known if a similar framework substitution could occur in Ba_8Si_{46}. For the aforementioned Ge clathrate, the Li was introduced from the LiGe precursor used in the synthesis. The synthesis of $Ba_{8-y}Si_{46}$ was reported from the oxidation of $Ba_4Li_2Si_6$, but neither Li substitution nor Si vacancies were observed in the products.[25]

The formation energy was calculated for the clathrate structure in which Li substituted Si in each of the 6c sites, resulting in a composition of $Ba_8Li_6Si_{40}$. The formation energy for this compound was −0.168 eV/atom, slightly higher than that calculated for $Ba_8Al_6Si_{40}$ (−0.175 eV/atom). The lattice constants were 10.57 and 10.51 Å for the Li- and Al-substituted compounds, respectively. From these results, we can see that Li framework substitution in Ba_8Si_{46} is energetically feasible.

3.2. Lithium Occupation of Empty Si_{20} and Si_{24} Cages. Despite the number of type I clathrates that have been synthesized,[18,47] Li is the only metal that has not been reported as a guest atom, presumably because the Li atoms are too small. Correlation diagrams for silicon clathrates[48] show that the free radius of a cage corresponds to the shortest M−Si bond distance minus the average radius of Si. With a covalent radius[43] of only 1.28 Å, Li is much smaller than Na (1.66 Å), the latter which can form both type I and type II structures. A similar analysis based on the sizes of the guest atoms and polyhedra cavities suggested that Li may be stable in type I clathrates made of carbon frameworks but not silicon.[8] Hence, the compound Li_8Si_{46}, with all 2a and 6d sites occupied by Li, may be hypothetical. This is consistent with the calculated positive formation energy of 0.044 eV/atom, although the slightly lower formation energy compared to guest-free Si_{46} (0.064 eV/atom) and smaller lattice constant (Figure 2b) showed the Li atoms provided some stabilizing effect. Similar phenomena were observed in calculations performed on guest-free type II clathrate Si_{136}.[20,21]

For the Ba-deficient clathrate Ba_6Si_{46}, Li occupation of the 2a sites to form $Li_2Ba_6Si_{46}$ was found to lower the formation energy, likely due to the increased stabilization imparted by the filling of the polyhedra cavities. Mixed guest atom clathrates have been experimentally observed, although not with Li, e.g., $Na_{2.9}Ba_{4.5}Si_{46}$[49] and $Sr_{0.7}Ba_{7.3}Al_{14}Si_{31}$.[50] The negative formation energy (−0.102 eV/atom) calculated for $Li_2Ba_6Si_{46}$ suggests that it is energetically feasible for Li to occupy the vacant Ba sites. The calculated lattice constant for $Li_2Ba_6Si_{46}$ did not change compared to Ba_6Si_{46} (Figure 2b). When substituting Si with Al on the framework, the formation energy decreased further to −0.150 eV/atom for $Li_2Ba_6Al_6Si_{40}$, indicating that the lithiated structure is more energetically favorable when Al-framework substitution is employed. Therefore, it is of importance to check the dynamical stability of the Al-containing clathrates. As an example, we calculated the phonon dispersion curve of $Li_2Ba_6Al_6S_{40}$ as shown in Figure S1. The absence of imaginary phonon frequencies throughout the entire Brillouin zone of the calculated phonon spectrum confirmed that the structure is dynamically stable.

3.3. Lithium Centered on the Hexagonal Faces of the Si_{24} Cages. The Si_{24} cages contain hexagonal faces in which the Si−Si bond angles are close to 120°, as opposed to the normal tetrahedral bond angle of 109.5°. The hexagons are connected through the Si 6c sites along the [100] direction, with every other hexagon rotated by 90°. The centers of these hexagonal faces, the 6b sites, are found on either side of the Ba 6d sites between adjacent Si_{24} cages (Figure 1b). These 6b sites are typically not occupied in type I silicon clathrate structures, presumably because typical guest atoms (e.g., Na, Ba, K) are too large. For Ba_8Si_{46}, a single Li atom was placed on one hexagonal face (6b site) to form $LiBa_8Si_{46}$. In this configuration, we found that the formation energy was −0.091 eV/atom, slightly higher than the formation energy for Ba_8Si_{46} (−0.116 eV/atom). This configuration also slightly increased the lattice constant by about 0.1 Å compared to that of Ba_8Si_{46}.

Next, full occupancy of the 6b sites ($x = 6$) was considered for Ba_6Si_{46}, Ba_8Si_{46}, and $Ba_6Al_6Si_{40}$. In all three cases, the formation energies became positive (Figure 2a) and the volume increased relative to the unlithiated compounds (Figure 2c). This is expected since the Li−Si bond distances on the hexagonal faces are much shorter (~2.5 Å) than those calculated when Li is in the 2a site inside the Si_{20} cage (3.3−3.4 Å). The advantage of using the Al-framework substitution is that the volume change is smaller upon lithiation. The volume increased ~6% for both Ba_6Si_{46} and Ba_8Si_{46} upon insertion of 6 Li. In contrast, the smaller change in lattice constant of only 1.4% between $Ba_6Al_6Si_{40}$ and $Li_6Ba_6Al_6Si_{40}$ meant that only a 4.4% change in volume was calculated.

Structures with Li in both 2a and 6b sites were also considered. For Ba_6Si_{46} and $Ba_6Al_6Si_{40}$, the structure for insertion of 5 Li ($x = 5$) was calculated with Li in both 2a sites and one-half of the 6b sites, whereas the $x = 8$ case had full Li occupancy in both sites. The Li sites and occupancies are summarized in Table S1. For both clathrates, the formation energies for $x = 5$ and 8 were lower than for $x = 6$ (Figure 2a). This suggests that the clathrates are more stable when the 2a sites are occupied. For $x = 8$, the only negative formation energy calculated was for $Li_8Ba_6Al_6Si_{40}$. This result shows the stabilizing role of the Al-framework substitution. The lattice constant also did not change much between $x = 6$ and $x = 8$, as expected since the additional 2 Li were placed inside the Si_{20} cage cavities. All of the bond distances increased when Al was substituted into $Li_8Ba_6Si_{46}$, as shown in Table 1.

Table 1. Comparison of Bond Distances (Angstroms) in $Li_8Ba_6Si_{46}$ and $Li_8Ba_6Al_6Si_{40}$, with Li in the 2a and 6b Sites

Li site	bond	$Li_8Ba_6Si_{46}$	$Li_8Ba_6Al_6Si_{40}$
on the hexagonal face (6b)	Li−Si(24k)	2.50	2.51
	Li−Si/Al(6c)	2.63	2.65
	Li−Ba	2.63	2.65
inside the Si_{20} cage (2a)	Li−Si	3.35, 3.43	3.37, 3.38

3.4. Lithium in off-Centered Pentagonal and Hexagonal Faces of the Si_{24} Cages. Several other locations for Li within the Si_{24} cages were investigated. We considered that the Li could sit within the plane of a hexagonal or pentagonal face or it could be off-plane such that it was not bisected by the face. The Li could also be centered within the polygon (i.e.,

DOI: 10.1021/acs.jpcc.5b07523
J. Phys. Chem. C 2015, 119, 28247−28257

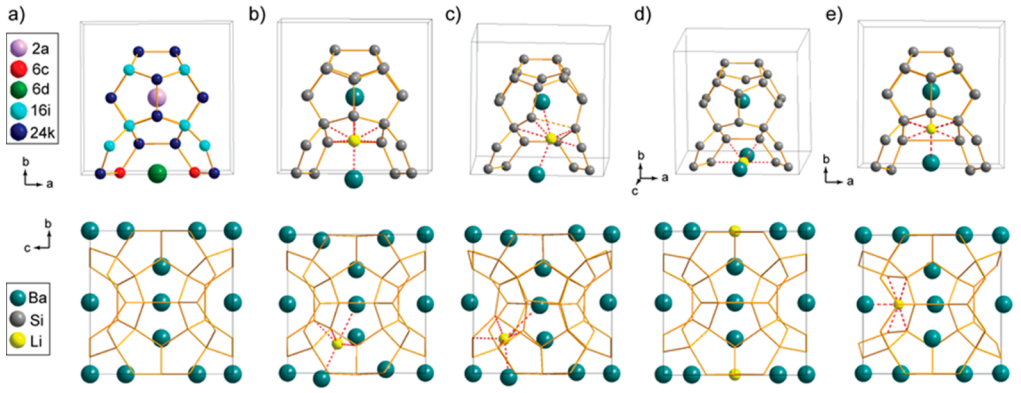

Figure 3. Structures of calculated $LiBa_8Si_{46}$ configurations with Li within the (a–d) Si_{24} cage or (e) Si_{20} cage. (Top row) View along the *c* axis for part of the Si_{24} and Si_{20} cages, with other atoms omitted for clarity. (Bottom row) Unit cell along the *a* axis. Li–Si and Li–Ba bonds are indicated with red dotted lines. (a) Li-free Ba_8Si_{46}, Wyckoff sites colored as follows: Ba 6d (green), Ba 2a (pink), Si 6c (red), Si 16i (cyan), Si 24k (blue); (b) Li_1-1, (c) Li_1-2, (d) Li_1-3, (e) Li_1-4.

equidistant from the closest Si atoms) or off-centered. These calculations were performed using Ba_8Si_{46} (Figure 3a) as the starting compound and adding a single Li atom to form $LiBa_8Si_{46}$, with the Li on the pentagonal faces (in the center, close to the Si atoms, or close to the middle of the Si–Si bonds), off-centered within a hexagonal plane, or off-plane of the hexagonal and pentagonal faces (Figure S2). From the seven different initial structures studied (Figure S2), three final lowest energy configurations were obtained (Figure 3b–d), which we designate Li_1-1, Li_1-2, and Li_1-3. The formation energies and lattice constants for the relaxed structures are shown in Table 2, and select bond distances and angles are presented in Figure S3 and Table S2. The interatomic distances and angles calculated for Ba_8Si_{46} were in close agreement with those derived experimentally.[23]

Table 2. Lattice Constants and Formation Energies for Calculated $LiBa_8Si_{46}$ Configurations

configuration	Li site description	lattice constant (Å)	formation energy (eV/atom)	volume increase (%)
Li_1-1	pentagonal off-plane, inside Si_{24} cage	10.47	−0.087	2.04
Li_1-2	bridge of 2 pentagons, inside Si_{24} cage	10.46	−0.087	1.72
Li_1-3	6b site, center of hexagonal face between adjacent Si_{24} cages	10.49	−0.091	2.49
Li_1-4	bridge of 2 pentagons, inside Si_{20} cage	10.48	−0.080	2.33

The results showed that the local energy minimum for Li around the pentagonal faces was in a 5-fold coordination slightly off-plane such that the Li atom was inside the Si_{24} cage. This is shown as configuration Li_1-1 (Figure 3b). This configuration resulted in a formation energy of −0.087 eV/atom. The bond distance between the Ba in the 2a and 6d sites increased from 5.81 Å in Ba_8Si_{46} to 6.23 Å, while the distance between two Ba 6d sites decreased slightly from 5.20 to 4.94 Å. The distance between Li and Si was on average 2.43 Å, smaller than the Li–Ba distances (2.92 and 3.31 Å). The main changes to the Si framework compared to the Li-free configuration were increases in the Si 16i–24k and 24k–24k bond lengths and corresponding bond angle changes for the distorted pentagonal face closest to the Li (Figure S3a–d).

If the Li were placed too close to a 16i–24k (Si–Si) bond, the Si pentagons became even more distorted, resulting in configuration Li_1-2 (Figure 3c). The Li was oriented near the Si 16i–24k bond bridging two adjacent pentagons, as shown in Figure S3e. The Li in this position caused reduction in the Si 24k–16i–24k bond angle from ∼110° in Ba_8Si_{46} to ∼90° in configuration Li_1-2, as illustrated in Figure S3b and S3f, respectively. The distortion placed the Li at the bottom point of a hexagonal plane with 5 Si atoms from the Si_{20} cage (Figure 3c). The formation energy for this configuration was −0.087 eV, similar to the Li_1-1 configuration described above. From the data in Table S2, it is apparent that in Li_1-2, the average Li–Ba and Li–Si (2.84 Å) bond distances are longer than in Li_1-1 due to the distortion.

The final configuration, Li_1-3, had the lowest formation energy and corresponded to Li centered in the center of the hexagon face, i.e., the 6b site, which was already described previously. This was the preferred location if the initial structure consisted of Li bisected by a hexagonal plane and in close proximity to a Si atom. However, if the Li was off-plane of the hexagonal face inside the Si_{24} cage and also off-centered, the preferred structure was configuration Li_1-1 (Figure S2). Comparing the bond distances of Li_1-3 with those in the Li_1-2 configurations, the average Si–Si (2.63 Å) and Li–Ba distances are smaller, but both Ba–Ba distances increased to >6 Å, with the 6d–6d length as large as 6.38 Å. This is consistent with an overall expansion of the lattice constant while maintaining a highly symmetric structure.

3.5. Lithium in off-Centered Pentagonal Face of the Si_{20} Cages. To investigate the structural effect of putting Li inside the smaller Si_{20} cage, three additional configurations were investigated. A single Li atom was placed inside the Si_{20} cage, both off-plane but either centered (Figure S5a) or off-centered (Figure S5b) with respect to the pentagonal face. After relaxation, both of these initial configurations formed lowest energy structures that were actually the same as configuration Li_1-1, with the Li atom shifted to the Si_{24} cage off-plane of a pentagonal face. On the other hand, when placing a single Li atom such that it bridged the 24k–24k (Si–Si) bond of two adjacent pentagonal faces (Figure S5c), it remained within the Si_{20} cage after relaxation, albeit with large bond length and bond angle distortion. Select bond lengths and angles within the Si_{20} cage are compared for Ba_8Si_{46} and this configuration of $LiBa_8Si_{46}$, which we designate Li_1-4, in Figure S6 and Table S2.

DOI: 10.1021/acs.jpcc.5b07523
J. Phys. Chem. C 2015, 119, 28247–28257

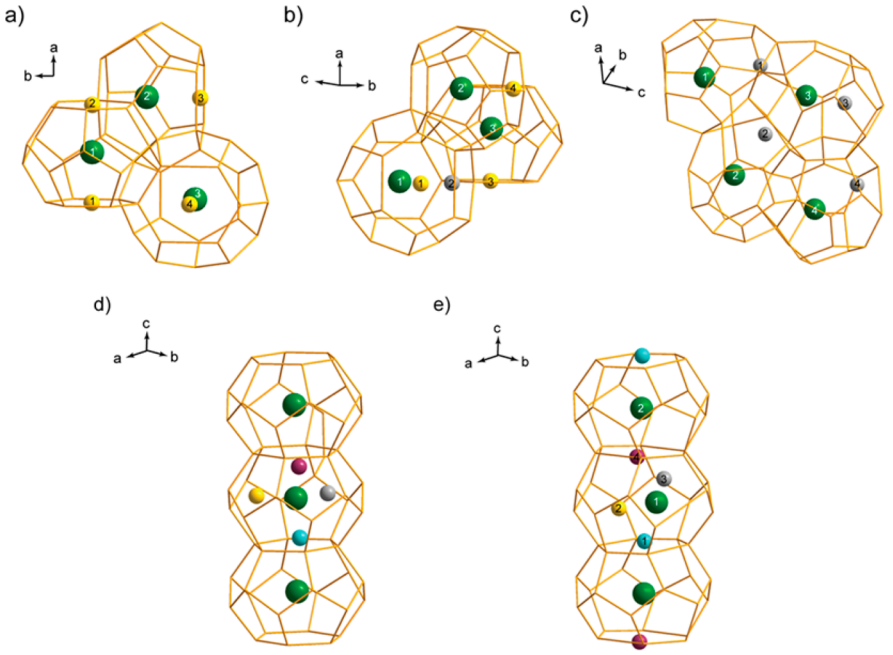

Figure 4. Structures of calculated $Li_4Ba_8Si_{46}$ configurations. Ba atoms are shown in green. (a–c) Li in the 6b sites are yellow spheres, and Li in the off-plane pentagonal sites are gray spheres. Certain cages containing only Ba are omitted for clarity. (a) Li_4-1, (b) Li_4-2, (c) Li_4-3; (d) initial (unrelaxed) and (e) final relaxed structure for Li_4-4, showing a Si_{24} chain along the *c* axis with the four Li atoms in different colors.

After relaxation, the largest change in bond length was the 24k–24k bond, which increased from 2.49 to 4.26 Å to accommodate for the presence of Li. The Li–Si bond distances ranged from 2.28 to 2.87 Å. These results suggest that Li does not prefer to remain inside the Si_{20} cage and will instead induce structural distortion to the cage framework or shift to the Si_{24} site off-centered of a pentagonal face.

3.6. Multiple Lithium Atoms Inside Si_{24} Cages. To study the structural effect of multiple Li atoms inside the clathrate cages, we first considered several possibilities to obtain $Li_4Ba_8Si_{46}$ (Figure 4).

- Configuration Li_4-1 (Figure 4a): Li atoms were placed in four 6b sites (center of hexagonal face).
- Configuration Li_4-2 (Figure 4b): Three Li atoms were placed in the 6b sites, and one Li atom was placed off-center of a pentagonal face (i.e., as in configuration Li_1-1 from Figure 3b).
- Configuration Li_4-3 (Figure 4c): Four Li atoms were placed in the pentagonal off-plane positions inside four adjoining Si_{24} cages.
- Configuration Li_4-4 (Figure 4d): Four Li atoms were placed together inside a single Si_{24} cage occupied by Ba to form a $BaLi_4$ cluster.

Due to uncertainties in the location of the Li atoms within the clathrate structures, higher degrees of lithiation were not calculated.

The lattice constants and formation energies for the relaxed structures are shown in Table 3. All of these configurations had negative formation energies, with configuration Li_4-3 showing the lowest energy. Both Li_4-3 and Li_4-3 structures, which involved putting Li and Ba inside the same cages, showed the greatest increases in lattice constant, distortion to the pentagonal and hexagonal faces, as well as shifts in the Ba location away from the cage centers. This was particularly pronounced for Li_4-4, in which a distorted trigonal pyramid was formed consisting of Ba and two Li in the equatorial positions, with the remaining two Li in the axial positions (Figure 4e). The calculated Ba–Li bond distances for the different $Li_4Ba_8Si_{46}$ configurations are listed in Table S3.

Table 3. Lattice Constants and Formation Energies for Calculated for $Li_4Ba_8Si_{46}$ Configurations

configuration	site description	no. of Li	lattice constant (Å)	formation energy (eV/atom)	volume increase (%)
Li_4-1	6b site	4	10.60	−0.033	5.81
Li_4-2	6b site	3	10.61	−0.052	6.18
	pentagonal off-plane	1			
Li_4-3	pentagonal off-plane	4	10.67	−0.062	7.92
Li_4-4	$BaLi_4$ cluster inside Si_{24} cage	4	10.69	−0.058	8.54

3.7. Average Equilibrium Lithium Voltage and Theoretical Capacities. The Gibbs free energy change for the reaction with lithium was calculated for Si_{46}, Ba_6Si_{46}, $Ba_6Al_6Si_{40}$, and Ba_8Si_{46}. For the clathrates containing empty cages, $\Delta G_r < 0$, which resulted in positive lithiation voltages, as shown in Table 4. This indicates that these materials will act as cathodes in half-cells containing Li counter electrodes and be lithiated during the discharge. Hence, the clathrates would act as suitable anodes when paired with a cathode such as $LiCoO_2$ or $LiFePO_4$ in a full cell. The presence of Ba guest atoms inside Si_{46} increased the lithiation voltage from 0.07 to 0.58 V vs Li/Li^+. The voltage in $Ba_6Al_6Si_{40}$ was slightly lower, suggesting that framework substitution with Al decreases the lithiation voltage. This is consistent with our previous experimental results on $Ba_yAl_zSi_{46-z}$ ($y < 8$; $8 < z < 11$), where lithiation of the clathrates was observed <0.5 V vs Li/Li^+.[30]

On the other hand, all of the different $LiBa_8Si_{46}$ and $Li_4Ba_8Si_{46}$ configurations studied had $\Delta G_r > 0$ and negative equilibrium lithium voltages (Table 4). These results indicate

DOI: 10.1021/acs.jpcc.5b07523
J. Phys. Chem. C 2015, 119, 28247–28257

Table 4. Calculated Gibbs Free Energy Change and Equilibrium Lithium Voltage for Lithium Insertion into Si_{46}, Ba_6Si_{46}, $Ba_6Al_6Si_{40}$, and Ba_8Si_{46}

reaction		ΔG_r, Gibbs free energy change for Li insertion (eV)	average lithiation voltage (V)
$Si_{46} + 8Li \rightarrow Li_8Si_{46}$		−0.583	0.07
$Ba_6Si_{46} + 2Li \rightarrow Li_2Ba_6Si_{46}$		−1.164	0.58
$Ba_6Al_6Si_{40} + 2Li \rightarrow Li_2Ba_6Al_6Si_{40}$		−1.101	0.55
$Ba_8Si_{46} + Li \rightarrow LiBa_8Si_{46}$	Li_1-1	1.455	−1.46
	Li_1-2	1.457	−1.46
	Li_1-3	1.231	−1.23
	Li_1-4	1.867	−1.87
$Ba_8Si_{46} + 4Li \rightarrow Li_4Ba_8Si_{46}$	Li_4-1	4.375	−1.09
	Li_4-2	3.274	−0.82
	Li_4-3	2.676	−0.67
	Li_4-4	2.875	−0.72

that formation of $LiBa_8Si_{46}$ and $Li_4Ba_8Si_{46}$ by lithiation of Ba_8Si_{46} would require external bias, i.e., charging, but that the reverse reaction (delithiation of $LiBa_8Si_{46}$ and $Li_4Ba_8Si_{46}$) would be spontaneous. The negative formation energies for $LiBa_8Si_{46}$ and $Li_4Ba_8Si_{46}$ (Figure 2a) indicate that these compounds are thermodynamically stable and can be formed from the bulk elements, but the positive Gibbs free energy change for the lithium insertion reaction suggests that their use as anodes in full cells would be limited. This is likely due to the full cage occupancy in Ba_8Si_{46}, whereas the Ba-deficient clathrates are stabilized when Li occupies the empty polyhedra, which provides a driving force for lithiation during the discharge. These results are also consistent with our previous experimental observations on electrochemical lithiation in Ba-deficient clathrates.[30] We note that the large variation in the calculated voltage depending on which structural configuration was used highlights the importance of the Li site on the expected lithiation voltage and that the configurations chosen here may not be representative of the structures observed experimentally.

Table S4 shows the calculated theoretical capacities for the lithiated compounds calculated using eq 8 for compositions up to $x = 8$. For Li_8Si_{46}, a theoretical capacity of 166 mAh/g was obtained, while capacities around 101 mAh/g are possible for both $Li_8Ba_6Si_{46}$ and $Li_8Ba_6Al_6Si_{40}$. Although the capacities are similar for the latter two compounds, substitution of the Si framework with Al showed lower formation energies (Figure 2a), pointing to the advantage of using Al-framework substitution. While these capacities are still much lower than those observed in graphite (~370 mAh/g) and conventional silicon anodes (~3000 mAh/g), we note that the observation that it is energetically feasible for multiple guest atoms to be placed in the Si_{24} cages has important implications for the application of type I clathrates as energy storage materials, since it increases the number of possible sites available other than solely in the center of the cage cavities. Recent experimental studies have found that Na dimer clusters can be formed in type II clathrate by tuning the synthetic conditions, with Na−Na bond distances of 2.74 Å measured at 10 K.[51] Furthermore, our experimental studies on $Ba_8Al_zSi_{46-z}$ showed that up to 44 Li per unit cell could be inserted without discernible changes to the clathrate structure,[30] with discharge capacities > 300 mAh/g achieved. Such a high lithiation capacity could be possible with the formation of clusters within the cage cavities. More structural information on the lithiated clathrate structures obtained experimentally will better elucidate the theoretical limits for the gravimetric capacities.

3.8. Electronic Structures and Density of States. The calculated band structures and density of states (DOS) for some of the type I clathrate structures discussed before are shown in Figure 5, while the total and projected DOS (PDOS) are shown in Figure 6. The results for Si_{46}, Ba_8Si_{46}, and $Ba_8Al_6Si_{40}$ are similar to those reported previously.[42,52] A direct band gap of 1.31 eV was calculated for Si_{46} (Figure 5a), which is slightly underestimated by DFT, whereas the clathrates

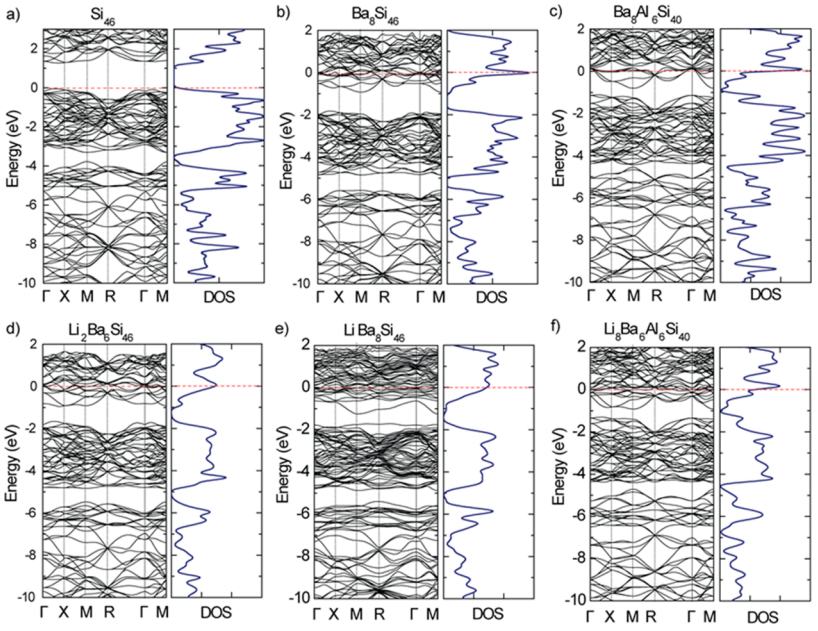

Figure 5. Band structure and density of states (DOS) for (a) Si_{46}, (b) Ba_8Si_{46}, (c) $Ba_8Al_6Si_{40}$, (d) $Li_2Ba_6Si_{40}$ (with Li in the 2a sites in the center of the Si_{20} cages), (e) $LiBa_8Si_{46}$ (Li_1-2 configuration), and (f) $Li_8Ba_6Al_6Si_{40}$ (Li in the 2a and 6b sites).

DOI: 10.1021/acs.jpcc.5b07523
J. Phys. Chem. C 2015, 119, 28247−28257

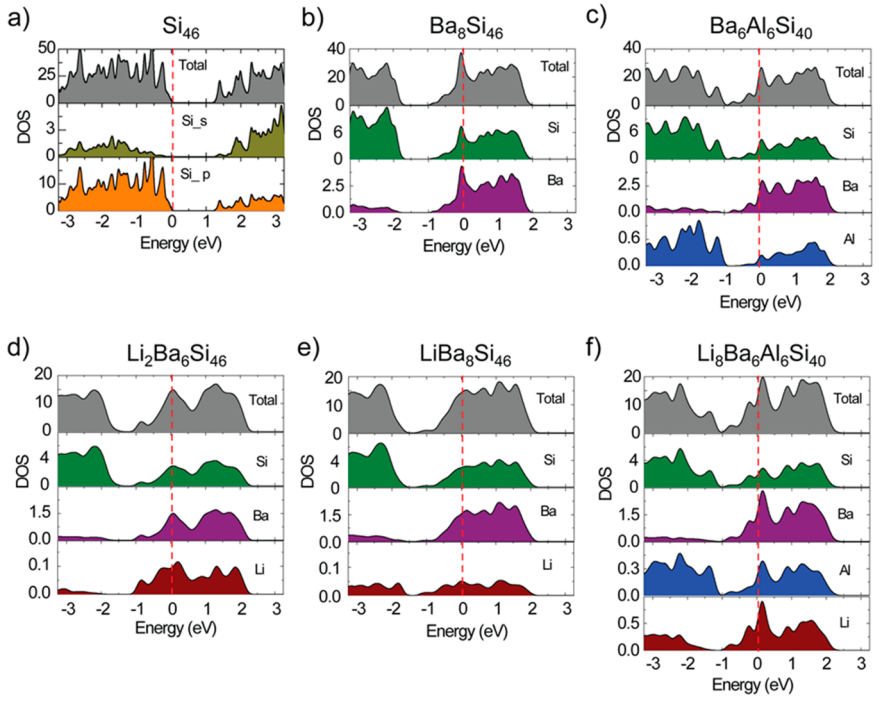

Figure 6. Total and projected DOS (states/eV per unit cell) for (a) Si_{46}, (b) Ba_8Si_{46}, (c) $Ba_8Al_6Si_{40}$, (d) $Li_2Ba_6Si_{40}$ (with Li in the 2a sites in the center of the Si_{20} cages), (e) $LiBa_8Si_{46}$ (Li_1-2 configuration), and (f) $Li_8Ba_6Al_6Si_{40}$ (Li in the 2a and 6b sites).

containing guest atoms were all metallic (Figure 5b–f). For clathrate materials, the electropositive guest atoms transfer valence electrons to the framework in an ionic-type host–guest interaction. For example, Ba_8Si_{46} will have an excess of 16 electrons from the 8 divalent Ba guest atoms, which become conduction electrons.[3] Substitution of silicon with a trivalent metal such as Al or Ga will allow for the electrons originating from the cage guest to be used to balance the charge through Zintl anions. Substitution of Si with Al will lead to charge balance at the Zintl condition in the compound $Ba_8Al_{16}Si_{30}$, whereby the 16 Al atoms can form four-bonded Zintl anions.[53] In cases where the amount of Al substitution is not sufficient to reach the Zintl condition, e.g., in $Ba_8Al_6Si_{40}$, the clathrate will remain metallic in nature.

Our calculated band structure for Ba_8Si_{46} showed a high DOS peak at the Fermi level (Figure 5b), which is predominately due to the hybridization of the Si_{46} conduction band with the orbitals from the Ba in the Si_{24} cages.[23] The PDOS for Ba_8Si_{46} (Figure 6b) shows that the Ba valence electrons contribute to the bottom of the conduction band. For the Al-substituted clathrate, introduction of Al shifts the Fermi level down compared to Ba_8Si_{46}.

To understand how the presence of Li inside the clathrate cage would affect the electronic structure, $Li_2Ba_6Si_{40}$ and $LiBa_8Si_{46}$ were investigated. As shown in Figure 6d and 6e, the presence of Li introduced more electrons to the bottom of the conduction band but without strong hybridization with the Ba or Si orbitals. This can be explained by the long bond distances between the Li and the Ba or Si in these structures. In $Li_2Ba_6Si_{46}$, the Li occupy the centers of the 2a sites in the Si_{20} cages normally occupied by Ba. The 2a–6b bond distance representing the Li–Ba bond length in this case is ~5.76 Å. For $LiBa_8Si_{46}$, in which the Li is off-center of a pentagonal face in a Si_{24} cage (the Li_1-2 configuration in Figure 3), the Li is 3.11 Å from the Ba in the 6d site (Table S2).

On the other hand, comparing the PDOS of $Ba_8Al_6Si_{40}$ (Figure 6c) with that of the lithiated version $Li_8Ba_6Al_6Si_{40}$ (Figure 6f) indicates hybridization between Li, Ba, and Al. This occurs because the Li in the 6b sites are in closer proximity to the Al in the 6c sites and Ba in the 6d sites (Figure S7). The calculated bond distances for Li–Ba and Li–Al (6c) were ~2.65 Å, and that for Li–Si (24k) was ~2.51 Å. The strong hybridization of Ba electrons with the Si_{46} conduction band and the high DOS close to the Fermi level are said to play key roles in the origin of superconductivity in Ba_8Si_{46} and $Na_2Ba_6Si_{46}$ at <8 K.[42,54] The similar features observed in the lithiated compounds suggest that they too may also display superconductivity properties, but this would require experimental verification.

To determine if there was significant electron transfer between the guest atoms and silicon clathrate framework, we analyzed the atomic charges in $Li_8Ba_6Si_{46}$ and $Li_8Ba_6Al_6Si_{40}$ as examples using the Bader scheme.[39] In the PAW potential provided by the simulation code, Li, Ba, and Si have 3, 10, and 4 valence electrons, respectively. The calculated average atomic charges of Li, Ba, and Si in $Li_8Ba_6Si_{46}$ were 2.21, 8.91, and 4.28, respectively, indicating some electron charge was transferred from the metal atoms to the Si framework. With partial Si substitution by Al, the average charges did not change much and were still 2.21 and 8.91 for Li and Ba in $Li_8Ba_6Al_6Si_{40}$.

4. DISCUSSION

From these data we can make the following conclusions regarding the energetically favored Li sites inside type I Ba-doped silicon clathrates and the implications for designing clathrate-based anodes for Li-ion batteries. Li occupation of defects in type I clathrates is a favorable process. Filling Ba-deficient structures (i.e., 2a site vacancies) with Li stabilizes the structures, as seen by the lower formation energies in Ba_6Si_{46} and $Ba_6Al_6Si_{40}$ for $x = 2$.

DOI: 10.1021/acs.jpcc.5b07523
J. Phys. Chem. C 2015, 119, 28247–28257

Li insertion into framework defects was also found to be favorable. Vacancy ordering on the 6c sites in type I germanium clathrates[55,56] has been observed and may be a promising way to create defined sites for Li in the framework. However, similar framework vacancies have not been observed in Si_{46}-based clathrates,[57] although framework defects have been proposed in group III substituted clathrates (e.g., $Ba_8Al_8Si_{36}\square_2$, where $\square$ is a vacancy)[58] as a means for charge compensation. It is also uncertain to what extent such framework vacancies can be utilized for charge storage, due to their limited concentration in stable silicon clathrate structures.

Framework substitution with Al to form ternary compounds is favorable for a number of reasons. As mentioned previously, there are practical advantages from a synthetic standpoint in that substitution of Si for Al enables the synthesis of the clathrates using thermal methods without requiring high pressures. Al substitution increases the lattice constant of the clathrate compared to the binary system, so that the volume increase upon lithiation is smaller, as shown in Figure 2c. Also, from previous neutron diffraction studies,[44] the Al framework substitution is rather disordered, which could increase the probability for vacancy formation and hence creation of additional sites for Li. For Ba_8Si_{46} and $Ba_6Al_6Si_{40}$, the additional Ba and presence of Al substitution, respectively, stabilize the lithiated structures for $x = 6$, although the energies were still slightly positive. Having the mixed Li occupation on the 2a and 6b sites ($x = 5$) was preferable and gave negative formation energies compared to the structure with six Li atoms on the hexagonal faces. This is likely due to the longer calculated Li−Si bond distances of 3.3−3.4 Å when Li was in the Si_{20} cage compared to 2.3−2.6 Å when Li was placed on the hexagonal faces. When both 2a and 6b sites in Ba_6Si_{46} were completely filled with Li ($x = 8$) the formation energy increased to 0.053 eV/atom. The stabilization effect of Al substitution could be observed, as $Li_8Ba_6Al_6Si_{40}$ had a formation energy of −0.011 eV/atom. These results, in addition to the simpler synthetic procedures, show that Al-substituted ternary silicon clathrate is preferred over the binary one. A recent study found a similar result in the analogous (yet still hypothetical) carbon clathrate system, wherein boron substitution of the carbon framework substantially lowered the enthalpic cost of inserting Li inside the structure,[59] suggesting that framework substitution may be a promising and general route for stabilizing Li-containing clathrates.

The guest atom spacing within the clathrate plays a significant role on the structure of the silicon framework after lithiation. In our previous work, we found that multiple Li atoms could be placed inside the Si_{28} cages of the type II clathrate $Na_{24}Si_{136}$.[20] The calculated Na−Li bond distances were 2.84−3.24 Å, which is a similar range as the calculated Li−Ba bond distances obtained for the different $LiBa_8Si_{46}$ structures studied here (Table S2). These results seem to point to a general trend in which the Li−M bond distances should be within a certain distance, considering not only the location of M within the same cage cavity but also the M in the adjacent cage. Additionally, if the Li is too close to the Si atoms, the Si−Si bond lengths will distort in order to maximize the Li−M distances. This is demonstrated in the $Li_4Ba_8Si_{46}$ structures in which the configuration with the most negative formation energy (Li_4-3) had the largest Li−Ba bond distances and most Si−Si bond length and bond angle distortion. Furthermore, the lowest energy structures for $LiBa_8Si_{46}$ suggest that Li prefers to occupy sites within the larger Si_{24} cavities over the Si_{20} ones.

In our calculations, the location of the Li can cause volume expansion and bond distortion that should be detectable using diffraction or spectroscopic techniques. The absence of such discernible changes in our previous studies could be due to the formation of metastable phases during the experimental lithiation processes, which are not captured by the DFT calculations performed here. Furthermore, we did not take into account the fact that clathrate guest atoms have been shown to display very different nuclear density (e.g., spherical vs torus shaped) with small changes in host structure and that disorder can cause off-centering of the guest from the centers of the cages.[53] It is also possible that experimentally, the Li atoms do not arrange in any ordered or symmetric fashion, while the structures calculated here considered discrete sites for the multiple Li atoms.

5. CONCLUSIONS

Density functional theory was used to investigate the effect of Li insertion into several Ba-doped type I silicon clathrate structures. The formation energy, lattice constant, volume change, and electronic structure were calculated. The sensitivity of the clathrate framework structure to changes upon Li insertion was highly dependent on the presence of Al-framework substitution, which can mitigate volume expansion, as well as the location of the Li atoms in the structure, namely, the distance away from other guest and framework atoms. Four low-energy configurations for $LiBa_8Si_{46}$ were identified. The calculated band structures and density of states (DOS) also showed that insertion of Li contributes electrons to the bottom of the conduction band, with stronger hybridization between Li, Ba, and Al orbitals when Li was in the hexagonal faces compared to inside the cage cavities.

■ ASSOCIATED CONTENT

Supporting Information

The Supporting Information is available free of charge on the ACS Publications website at DOI: 10.1021/acs.jpcc.5b07523.

Tables containing Li site occupancy in calculated structures, select calculated interatomic distances in Ba_8Si_{46}, $LiBa_8Si_{46}$, and $Li_4Ba_8Si_{46}$, and theoretical specific capacities for lithiated compounds; figures showing the calculated phonon dispersion spectrum for $Li_2Ba_6Al_6Si_{40}$, initial and final relaxed structures for $LiBa_8Si_{46}$, select Si−Si interatomic distances and bond angles for $LiBa_8Si_{46}$, distorted pentagonal faces in the Li_1-2 configuration of $LiBa_8Si_{46}$, and unit cell of $Li_8Ba_6Al_6Si_{40}$ (PDF)

■ AUTHOR INFORMATION

Corresponding Author

*E-mail: candace.chan@asu.edu.

Notes

The authors declare no competing financial interest.

■ ACKNOWLEDGMENTS

This work was supported using new faculty startup funds from the Fulton Schools of Engineering (C.K.C.) and a Faculty Scholarship from the College of Letters and Sciences (X.P.) at Arizona State University (ASU) as well as funding from NSF DMR 1206795 (C.K.C. and Y.L.). The authors would also like

DOI: 10.1021/acs.jpcc.5b07523
J. Phys. Chem. C 2015, 119, 28247−28257

to thank K. S. Chan, W. Liang, and M.A. Miller for helpful discussions.

REFERENCES

(1) Kasper, J. S.; Hagenmuller, P.; Pouchard, M.; Cros, C. Clathrate Structure of Silicon Na_8Si_{46} and Na_xSi_{136} ($x < 11$). *Science* **1965**, *150*, 1713−1714.

(2) Chan, K. S.; Miller, M. A.; Liang, W.; Ellis-Terrell, C.; Peng, X. First-Principles Computational Design and Synthesis of Hybrid Carbon−Silicon Clathrates. *J. Mater. Sci.* **2014**, *49*, 2723−2733.

(3) Fukuoka, H.; Kiyoto, J.; Yamanaka, S. Superconductivity of Metal Deficient Silicon Clathrate Compounds, $Ba_{8-x}Si_{46}$ ($0 < x \leq 1.4$). *Inorg. Chem.* **2003**, *42*, 2933−2937.

(4) Reny, E.; San Miguel, A.; Guyot, Y.; Masenelli, B.; Mélinon, P.; Saviot, L.; Yamanaka, S.; Champagnon, B.; Cros, C.; Pouchard, M.; et al. Vibrational Modes in Silicon Clathrate Compounds: A Key to Understanding Superconductivity. *Phys. Rev. B: Condens. Matter Mater. Phys.* **2002**, *66*, 014532.

(5) Connétable, D.; Timoshevskii, V.; Masenelli, B.; Beille, J.; Marcus, J.; Barbara, B.; Saitta, A.; Rignanese, G. M.; Mélinon, P.; Yamanaka, S.; et al. Superconductivity in Doped sp^3 Semiconductors: The Case of the Clathrates. *Phys. Rev. Lett.* **2003**, *91*, 247001.

(6) Condron, C. L.; Martin, J.; Nolas, G. S.; Piccoli, P. M. B.; Schultz, A. J.; Kauzlarich, S. M. Structure and Thermoelectric Characterization of $Ba_8Al_{14}Si_{31}$. *Inorg. Chem.* **2006**, *45*, 9381−9386.

(7) Tsujii, N.; Roudebush, J. H.; Zevalkink, A.; Cox-Uvarov, C. A.; Snyder, G. J.; Kauzlarich, S. M. Phase Stability and Chemical Composition Dependence of the Thermoelectric Properties of the Type-I Clathrate $Ba_8Al_xSi_{46-x}$ ($8 \leq x \leq 15$). *J. Solid State Chem.* **2011**, *184*, 1293−1303.

(8) Karttunen, A. J.; Fässler, T. F.; Linnolahti, M.; Pakkanen, T. A. Structural Principles of Semiconducting Group 14 Clathrate Frameworks. *Inorg. Chem.* **2011**, *50*, 1733−1742.

(9) Chan, K. S.; Miller, M. A.; Liang, W.; Ellis-Terrell, C. Computational Design and Synthesis of Nitrogen-Substituted Carbon and Silicon Clathrates. *Mater. Res. Lett.* **2014**, *2*, 70−75.

(10) Nataraj, D.; Nagao, J. Structure and Raman Scattering Study on $Ba_8Ga_xSi_{46-x}$ (x = 10 and 16) Type I Clathrates. *J. Solid State Chem.* **2004**, *177*, 1905−1911.

(11) Neiner, D.; Okamoto, N. L.; Condron, C. L.; Ramasse, Q. M.; Yu, P.; Browning, N. D.; Kauzlarich, S. M. Hydrogen Encapsulation in a Silicon Clathrate Type I Structure: $Na_{5.5}(H_2)_{2.15}Si_{46}$: Synthesis and Characterization. *J. Am. Chem. Soc.* **2007**, *129*, 13857−13862.

(12) Neiner, D.; Okamoto, N. L.; Yu, P.; Leonard, S.; Condron, C. L.; Toney, M. F.; Ramasse, Q. M.; Browning, N. D.; Kauzlarich, S. M. Synthesis and Characterization of $K_{8-x}(H_2)_ySi_{46}$. *Inorg. Chem.* **2010**, *49*, 815−822.

(13) Obrovac, M. N.; Christensen, L. Structural Changes in Silicon Anodes During Lithium Insertion/Extraction. *Electrochem. Solid-State Lett.* **2004**, *7*, A93.

(14) Hatchard, T. D.; Dahn, J. R. In Situ XRD and Electrochemical Study of the Reaction of Lithium with Amorphous Silicon. *J. Electrochem. Soc.* **2004**, *151*, A838.

(15) Chan, C. K.; Peng, H.; Liu, G.; McIlwrath, K.; Zhang, X. F.; Huggins, R. A.; Cui, Y. High-Performance Lithium Battery Anodes Using Silicon Nanowires. *Nat. Nanotechnol.* **2008**, *3*, 31−35.

(16) Miller, M. A.; Chan, K. S.; Liang, W.; Chan, C. K. Clathrate Allotropes for Rechargeable Batteries. U.S. Patent 8,906,551, 2014.

(17) Lü, Y. J. Homogeneous Two-Dimensional Nucleation of Guest-Free Silicon Clathrates. *Philos. Mag.* **2015**, *95*, 242−258.

(18) Nolas, G. S. *The Physics and Chemistry of Inorganic Clathrates*; Springer Netherlands: Dordrecht, 2014; Vol. *199*.

(19) Langer, T.; Dupke, S.; Trill, H.; Passerini, S.; Eckert, H.; Pöttgen, R.; Winter, M. Electrochemical Lithiation of Silicon Clathrate-II. *J. Electrochem. Soc.* **2012**, *159*, A1318−A1322.

(20) Wagner, N. A.; Raghavan, R.; Zhao, R.; Wei, Q.; Peng, X.; Chan, C. K. Electrochemical Cycling of Sodium-Filled Silicon Clathrate. *ChemElectroChem* **2014**, *1*, 347−353.

(21) Yang, J.; Tse, J. S. Silicon Clathrates as Anode Materials for Lithium Ion Batteries? *J. Mater. Chem. A* **2013**, *1*, 7782.

(22) Rachi, T.; Tanigaki, K.; Kumashiro, R.; Winter, J.; Kuzmany, H. Preparation and Electronic States of $Na_{16}Ba_8Si_{136}$ Clathrate. *Chem. Phys. Lett.* **2005**, *409*, 48−51.

(23) Kitano, A.; Moriguchi, K.; Yonemura, M.; Munetoh, S.; Shintani, A.; Fukuoka, H.; Yamanaka, S.; Nishibori, E.; Takata, M.; Sakata, M. Structural Properties and Thermodynamic Stability of Ba-Doped Silicon Type-I Clathrates Synthesized Under High Pressure. *Phys. Rev. B: Condens. Matter Mater. Phys.* **2001**, *64*, 045206.

(24) Yamanaka, S.; Enishi, E.; Fukuoka, H.; Yasukawa, M. High-Pressure Synthesis of a New Silicon Clathrate Superconductor, Ba_8Si_{46}. *Inorg. Chem.* **2000**, *39*, 56−58.

(25) Liang, Y.; Böhme, B.; Reibold, M.; Schnelle, W.; Schwarz, U.; Baitinger, M.; Lichte, H.; Grin, Y. Synthesis of the Clathrate-I Phase $Ba_{8-x}Si_{46}$ via Redox Reactions. *Inorg. Chem.* **2011**, *50*, 4523−4528.

(26) Fukuoka, H.; Kiyoto, J.; Yamanaka, S. Synthesis and Superconductivity of Barium Deficient Type I Silicon Clathrate Compounds, $Ba_{8-x}Si_{46}$. *J. Phys. Chem. Solids* **2004**, *65*, 333−336.

(27) Tanigaki, K.; Shimizu, T.; Itoh, K. M.; Teraoka, J.; Moritomo, Y.; Yamanaka, S. Mechanism of Superconductivity in the Polyhedral-Network Compound Ba_8Si_{46}. *Nat. Mater.* **2003**, *2*, 653−655.

(28) Eisenmann, B.; Schafer, H.; Zagler, R. Die Verbindungen $A_8^{II}B_{16}^{III}B_{30}^{IV}$ (A^{II} = Sr,Ba; B^{III} = Al,Ga; B^{IV} = Si,Ge,Sn) und ihre Kafigstrukturen. *J. Less-Common Met.* **1986**, *118*, 43−55.

(29) Aydemir, U.; Candolfi, C.; Ormeci, A.; Borrmann, H.; Burkhardt, U.; Oztan, Y.; Oeschler, N.; Baitinger, M.; Steglich, F.; Grin, Y. Synthesis, Crystal Structure, and Physical Properties of the Type-I Clathrate $Ba_{8-\delta}Ni_x\square_ySi_{46-x-y}$. *Inorg. Chem.* **2012**, *51*, 4730−4741.

(30) Li, Y.; Wagner, N. A.; Raghavan, R.; Davidowski, S. K.; Baggetto, L.; Zhao, R.; Cheng, Q.; Yarger, J. L.; Veith, G. M.; Ellis-Terrell, C.; et al. Type I Clathrates as Novel Silicon Anodes: An Electrochemical and Structural Investigation. *Adv. Sci.* **2015**, *2*, 1500057.

(31) Kresse, G.; Joubert, D. From Ultrasoft Pseudopotentials to the Projector Augmented-Wave Method. *Phys. Rev. B: Condens. Matter Mater. Phys.* **1999**, *59*, 1758.

(32) Kresse, G.; Furthmuller, J. Efficient Iterative Schemes for Ab Initio Total-Energy Calculations Using a Plane-Wave Basis Set. *Phys. Rev. B: Condens. Matter Mater. Phys.* **1996**, *54*, 11169−11186.

(33) Perdew, J. P.; Burke, K.; Ernzerhof, M. Generalized Gradient Approximation Made Simple. *Phys. Rev. Lett.* **1996**, *77*, 3865.

(34) Blake, N. P.; Bryan, D.; Latturner, S.; Møllnitz, L.; Stucky, G. D.; Metiu, H. Structure and Stability of the Clathrates $Ba_8Ga_{16}Ge_{30}$, $Sr_8Ga_{16}Ge_{30}$, $Ba_8Ga_{16}Si_{30}$, and $Ba_8In_{16}Sn_{30}$. *J. Chem. Phys.* **2001**, *114*, 10063.

(35) Nenghabi, E. N.; Myles, C. W. First Principles Calculations of the Structural, Electronic and Vibrational Properties of the Clathrates $Ba_8Al_{16}Ge_{30}$and $Ba_8Al_{16}Si_{30}$. *J. Phys.: Condens. Matter* **2008**, *20*, 415214.

(36) Norouzzadeh, P.; Myles, C. W.; Vashaee, D. Structural, Electronic, Phonon and Thermodynamic Properties of Hypothetical Type-VIII Clathrates Ba_8Si_{46} and $Ba_8Al_{16}Si_{30}$ Investigated by First Principles. *J. Alloys Compd.* **2014**, *587*, 474−480.

(37) Togo, A.; Oba, F.; Tanaka, I. First-Principles Calculations of the Ferroelastic Transition between Rutile-Type and $CaCl_2$-Type SiO_2 at High Pressures. *Phys. Rev. B: Condens. Matter Mater. Phys.* **2008**, *78*, 134106.

(38) Togo, A.; Tanaka, I. First Principles Phonon Calculations in Materials Science. *Scr. Mater.* **2015**, *108*, 1−5.

(39) Sanville, E.; Kenny, S. D.; Smith, R.; Henkelman, G. Improved Grid-Based Algorithm for Bader Charge Allocation. *J. Comput. Chem.* **2007**, *28*, 899−908.

(40) Aydinol, M. K.; Ceder, G. First-Principles Prediction of Insertion Potentials in Li-Mn Oxides for Secondary Li Batteries. *J. Electrochem. Soc.* **1997**, *144*, 3832−3835.

(41) Aydinol, M. K.; Kohan, A. F.; Ceder, G.; Cho, K.; Joannopoulos, J. Ab Initio Study of Lithium Intercalation in Metal Oxides and Metal Dichalcogenides. *Phys. Rev. B: Condens. Matter Mater. Phys.* **1997**, *56*, 1354−1365.

DOI: 10.1021/acs.jpcc.5b07523
J. Phys. Chem. C 2015, 119, 28247−28257

(42) Moriguchi, K.; Yonemura, M.; Shintani, A.; Yamanaka, S. Electronic Structures of $Na_8Si_{46}$and Ba_8Si_{46}. *Phys. Rev. B: Condens. Matter Mater. Phys.* **2000**, *61*, 9859−9862.
(43) Cordero, B.; Gómez, V.; Platero-Prats, A. E.; Revés, M.; Echeverría, J.; Cremades, E.; Barragán, F.; Alvarez, S. Covalent Radii Revisited. *Dalton Trans.* **2008**, 2832.
(44) Roudebush, J. H.; de la Cruz, C.; Chakoumakos, B. C.; Kauzlarich, S. M. Neutron Diffraction Study of the Type I Clathrate $Ba_8Al_xSi_{46-x}$: Site Occupancies, Cage Volumes, and the Interaction Between the Guest and the Host Framework. *Inorg. Chem.* **2012**, *51*, 1805−1812.
(45) Roudebush, J. H.; Tsujii, N.; Hurtando, A.; Hope, H.; Grin, Y.; Kauzlarich, S. M. Phase Range of the Type-I Clathrate $Sr_8Al_xSi_{46-x}$ and Crystal Structure of $Sr_8Al_{10}Si_{36}$. *Inorg. Chem.* **2012**, *51*, 4161−4169.
(46) Liang, Y.; Böhme, B.; Ormeci, A.; Borrmann, H.; Pecher, O.; Haarmann, F.; Schnelle, W.; Baitinger, M.; Grin, Y. A Clathrate-I Phase with Li-Ge Framework. *Chem. - Eur. J.* **2012**, *18*, 9818−9822.
(47) Bobev, S.; Sevov, S. C. Clathrates of Group 14 with Alkali metals: An Exploration. *J. Solid State Chem.* **2000**, *153*, 92−105.
(48) Cros, C.; Pouchard, M. Sur les Phases de Type Clathrate du Silicium et des Éléments Apparentés (C, Ge, Sn): Une Approche Historique. *C. R. Chim.* **2009**, *12*, 1014−1056.
(49) Kawaji, H.; Horie, H.; Yamanaka, S.; Ishikawa, M. Superconductivity in the Silicon Clathrate Compound $(Na,Ba)_xSi_{46}$. *Phys. Rev. Lett.* **1995**, *74*, 1427−1429.
(50) Condron, C. L.; Kauzlarich, S. M.; Nolas, G. S. Structure and Thermoelectric Characterization of $A_xBa_{8-x}Al_{14}Si_{31}$(A = Sr, Eu) Single Crystals. *Inorg. Chem.* **2007**, *46*, 2556−2562.
(51) Yamanaka, S.; Komatsu, M.; Tanaka, M.; Sawa, H.; Inumaru, K. High-Pressure Synthesis and Structural Characterization of the Type II Clathrate Compound $Na_{30.5}Si_{136}$ Encapsulating Two Sodium Atoms in the Same Silicon Polyhedral Cages. *J. Am. Chem. Soc.* **2014**, *136*, 7717−7725.
(52) Li, Y.; Garcia, J.; Chen, N.; Liu, L.; Li, F.; Wei, Y.; Bi, S.; Cao, G.; Feng, Z. S. Superconductivity in Al-substituted Ba_8Si_{46} Clathrates. *J. Appl. Phys.* **2013**, *113*, 203908.
(53) Christensen, M.; Johnsen, S.; Iversen, B. B. Thermoelectric Clathrates of Type I. *Dalton Trans.* **2010**, *39*, 978−992.
(54) Saito, S.; Oshiyama, A. Electronic Structure of Si_{46} and $Na_2Ba_6Si_{46}$. *Phys. Rev. B: Condens. Matter Mater. Phys.* **1995**, *51*, 2628−2631.
(55) Carrillo-Cabrera, W.; Budnyk, S.; Prots, Y.; Grin, Y. Z. Ba_8Ge_{43} Revisited: A 2a′ x 2a′ x 2a′ Superstructure of the Clathrate-I Type with Full Vacancy Ordering. *Z. Anorg. Allg. Chem.* **2004**, *630*, 2267−2276.
(56) Okamoto, N. L.; Oh, M. W.; Nishii, T.; Tanaka, K.; Inui, H. Crystal Structure and Thermoelectric Properties of the Type-I Clathrate Compound Ba_8Ge_{43} with an Ordered Arrangement of Ge Vacancies. *J. Appl. Phys.* **2006**, *99*, 033513.
(57) Ramachandran, G. K.; McMillan, P. F.; Dong, J.; Sankey, O. F. $K_{7.62(1)}Si_{46}$ and $Rb_{6.15(2)}Si_{46}$: Two Structure I Clathrates with Fully Occupied Framework Sites. *J. Solid State Chem.* **2000**, *154*, 626−634.
(58) Mudryk, Y.; Rogl, P.; Paul, C.; Berger, S.; Bauer, E.; Hilscher, G.; Godart, C.; Noël, H. Thermoelectricity of Clathrate I Si and Ge Phases. *J. Phys.: Condens. Matter* **2002**, *14*, 7991.
(59) Zeng, T.; Hoffmann, R.; Nesper, R.; Ashcroft, N. W.; Strobel, T. A.; Proserpio, D. M. Li-Filled, B-Substituted Carbon Clathrates. *J. Am. Chem. Soc.* **2015**, *137*, 12639−12652.

DOI: 10.1021/acs.jpcc.5b07523
J. Phys. Chem. C 2015, 119, 28247−28257